Author Manuscript

Author Manuscript

Author Manuscript

Author Manuscript

HHS Public Access

Author manuscript

Cancer Lett. Author manuscript; available in PMC 2022 August 30.

Published in final edited form as:

Cancer Lett. 2022 February 01; 526: 155–167. doi:10.1016/j.canlet.2021.11.016.

Giant obscurin regulates migration and metastasis via RhoA-dependent cytoskeletal remodeling in pancreatic cancer

Soontorn Tuntithavornwat[a,1], **Daniel J. Shea**[a,1], **Bin Sheng Wong**[a,b,1], **Talia Guardia**[c], **Se Jong Lee**[a], **Christopher L. Yankaskas**[a,b], **Lei Zheng**[d], **Aikaterini Kontrogianni-Konstantopoulos**[c,**], **Konstantinos Konstantopoulos**[a,b,d,e,*]

[a] Department of Chemical and Biomolecular Engineering, The Johns Hopkins University, Baltimore, MD, USA

[b] Institute for NanoBioTechnology, The Johns Hopkins University, Baltimore, MD, USA

[c] Department of Biochemistry and Molecular Biology, University of Maryland School of Medicine Marlene and Stewart Greenebaum Comprehensive Cancer Center, Baltimore, MD, USA

[d] Department of Oncology, The Johns Hopkins University School of Medicine, Baltimore, MD, USA

[e] Department of Biomedical Engineering, The Johns Hopkins University, Baltimore, MD, USA

Abstract

Obscurins, encoded by the *OBSCN* gene, are giant cytoskeletal proteins with structural and regulatory roles. Large scale omics analyses reveal that *OBSCN* is highly mutated across different types of cancer, exhibiting a 5–8% mutation frequency in pancreatic cancer. Yet, the functional role of *OBSCN* in pancreatic cancer progression and metastasis has to be delineated. We herein show that giant obscurins are highly expressed in normal pancreatic tissues, but their levels are markedly reduced in pancreatic ductal adenocarcinomas. Silencing of giant obscurins in non-tumorigenic Human Pancreatic Ductal Epithelial (HPDE) cells and obscurin-expressing Panc5.04 pancreatic cancer cells induces an elongated, spindle-like morphology and faster cell migration via cytoskeletal remodeling. Specifically, depletion of giant obscurins downregulates RhoA activity, which in turn results in reduced focal adhesion density, increased microtubule growth rate and faster actin dynamics. Although *OBSCN* knockdown is not sufficient to induce *de novo* tumorigenesis, it potentiates tumor growth in a subcutaneous implantation model and

* Corresponding author. The Johns Hopkins University, 3400 N. Charles Street, 114 Croft Hall, Baltimore, MD, 21218, USA. konstant@jhu.edu (K. Konstantopoulos). ** Corresponding author. University of Maryland School of Medicine, 108 N. Greene Street, BRF 215A, Baltimore, MD, 21201, USA. akontrogianni@som.umaryland.edu (A. Kontrogianni-Konstantopoulos).

[1] Co-first authors.

Author contributions

S.T., D.J.S. and B.S.W.: design, collection and assembly of *in vitro* data, data analysis and interpretation, manuscript writing; S.T., B.S.W., L.Z.: collection and assembly of *in vivo* data, data analysis and interpretation, manuscript writing; T.G.: generation of obscurin antibodies, Western Blot experiments, data collection and analysis, manuscript writing; S.J.L. and C.L.Y. performed select *in vitro* experiments, analyzed and interpreted data; A.K.K. and K.K.: conception and design, data analysis and interpretation, manuscript writing.

Declaration of competing interest

All authors declare that they have no relevant conflict of interest.

Appendix A. Supplementary data

Supplementary data to this article can be found online at https://doi.org/10.1016/j.canlet.2021.11.016.

Author Manuscript Author Manuscript Author Manuscript Author Manuscript

exacerbates metastasis in a hemispleen murine model of pancreatic cancer metastasis, thereby shortening survival. Collectively, these findings reveal a critical role of giant obscurins as tumor suppressors in normal pancreatic epithelium whose loss of function induces RhoA-dependent cytoskeletal remodeling, and promotes cell migration, tumor growth and metastasis.

Keywords

Cytoskeleton; Migration; Metastasis

1. Introduction

Pancreatic cancer is an extremely lethal malignancy with a 5-year survival rate of 9% [1]. Pancreatic ductal adenocarcinoma (PDAC) is the most prevalent type of pancreatic neoplasm, mainly originating from incipient premalignant lesions in the pancreas known as pancreatic intraepithelial neoplasias, following accumulation of multiple mutations over time [1,2]. Central to the poor prognosis of pancreatic cancer is delayed diagnosis due to the absence of noticeable and specific clinical symptoms in the early stages of the disease, the lack of sensitive imaging modalities to detect early neoplasias, and the paucity of reliable molecular biomarkers [3]. With the majority of PDAC patients being diagnosed when the tumor has either locally advanced to nearby arteries and veins or already metastasized to other organs [4] and is thus surgically unresectable, it is of paramount importance to understand the molecular etiologies of the disease initiation and progression.

Obscurins are giant cytoskeletal proteins with structural and regulatory roles which are encoded by the *OBSCN* gene that spans ~170 kb on human chromosome 1q42 [5–7]. *OBSCN* undergoes extensive alternative splicing, giving rise to multiple isoforms ranging in size between 40 and 870 kDa [5,8,9]. Although the molecular identity and expression profile of the small (40–260 kDa) and intermediate (260–600 kDa) obscurins are largely unknown, giant obscurins (720–870 kDa) have been extensively studied [10]. Giant obscurins, referred to as obscurin-A (~720 kDa) and obscurin-B (~870 kDa), are highly modular, consisting of tandem immunoglobulin (Ig) and fibronectin-III (FN-III) domains, followed by an array of signaling motifs, including a calmodulin-binding IQ motif and a tripartite cassette composed of a Src homology 3 (SH3) motif, a Rho-guanine nucleotide exchange factor (RhoGEF) motif, and a pleckstrin homology (PH) domain (Fig. 1A). Their extreme COOH-termini, however, diverge with obscurin-A containing a non-modular COOH-terminus that bears ankyrin-binding sites and obscurin-B containing two active Ser/Thr kinase domains that belong to the Myosin Light Chain Kinase (MLCK) family [10].

Although obscurins were originally identified in striated muscle cells [5], during the last decade it has become increasingly clear that they are expressed in non-muscle tissues too, where they play key roles in maintaining cell homeostasis [9,11]. This notion was instigated in a pioneering study where sequencing analysis of 13,023 genes in breast and colorectal cancers identified *OBSCN* as one of 189 candidate genes displaying somatic mutations at high frequency [12]. Further analysis of the mutational profile of the *OBSCN* gene revealed novel somatic mutations in melanoma and a germline mutation in glioblastoma

Author Manuscript Author Manuscript Author Manuscript Author Manuscript

[13], while analysis of whole genome arrays of gastrointestinal stromal and leiomyosarcoma tumors showed that the differential expression of *OBSCN* and *PRUNE2* (*C9orf65)* could be used as a reliable two-gene classifier to distinguish the two tumor types [14]. Since these original observations, extensive work from our group has indicated that giant obscurins possess tumor suppressor functions in breast epithelial cells [15,16], and that breast cancer patients with obscurin-deficient tumors exhibit significantly reduced overall and recurrence free survival. Consistent with these findings, *OBSCN* has been described as one among the 63 top mutated candidate driver genes in breast cancer with an average mutational rate of 11.4% [17,18], while changes in the *OBSCN* expression levels have been implicated as potential diagnostic markers for prostate cancer [19] and adrenocortical carcinoma [20]. Moreover, use of publicly available databases has indicated a 5–8% mutational frequency of *OBSCN* in pancreatic cancer (Supplementary Fig. 1A) with the majority being missense mutations spanning its entire length (Supplementary Fig. 1B). Consistent with this, *OBSCN* has been described as one of the most commonly mutated genes in pancreatic cancer with the identified mutations predicted to have damaging effects [21].

Given the poor prognosis of pancreatic cancer, our limited understanding about the molecular etiologies underlying the formation and progression of pancreatic tumors, and the high mutational prevalence of *OBSCN* in pancreatic cancer, we set forth to elucidate its functional role in pancreatic cancer progression and metastasis. Our studies demonstrate that human PDAC biopsies express significantly reduced levels of obscurins compared to matched controls. In accordance with this finding, loss of obscurins from pancreatic epithelial cells leads to altered RhoA signaling accompanied by cytoskeletal remodeling *in vitro*. Importantly, obscurin downregulation in pancreatic cancer cells potentiates tumor growth and metastasis leading to reduced survival *in vivo*. Together, our findings indicate that *OBSCN* is a potent tumor suppressor in pancreatic epithelial cells whose loss of function accelerates pancreatic cancer progression and metastasis, thereby shortening survival.

2. Materials and methods

2.1. Cell culture

SW1990, CFPAC-1 cells were purchased from the American Type Culture Collection. Human Pancreatic Ductal Epithelial (HPDE), Pa03C, Pa07C and Panc5.04 cells have been previously described [22,23]. HPDE cells were cultured in keratinocyte serum-free medium (SFM) supplemented with 30 μg/ml bovine pituitary extract, 0.1 ng/ml epidermal growth factor (EGF) (Gibco), and 50 μg/ml gentamicin. SW1990, CFPAC-1, Pa03C, Pa07C and Panc5.04 cells were cultured in standard DMEM (Gibco) with 10% Fetal Bovine Serum (FBS, Gibco) and either 50 μg/ml gentamicin (Sigma-Aldrich) or 1% penicillin/streptomycin (Gibco). AsPC-1 and Panc10.05 cells were cultured in RPMI1640 (Gibco) with 10% FBS and 1% penicillin/streptomycin. All cell lines were used for up to 10 passages after thawing from frozen stocks and were routinely tested for mycoplasma contamination via quantitative polymerase chain reaction (qPCR) [24]. The cell lines were not further authenticated. CFPAC-1 and Pa03c were isolated from liver metastases of pancreatic tumors; Pa07c

Author Manuscript Author Manuscript Author Manuscript Author Manuscript

and SW1990 from peritoneal and splenic metastases of pancreatic tumors, respectively; Panc5.04 and Panc10.05 from primary PDACs; AsPC-1 from ascites of a PDAC patient.

2.2. Generation of stable cell lines

Stable cell lines of scramble control and obscurin knockdown HPDE and Panc5.04 were generated with short hairpin RNA (shRNA) technology as previously described [23,24]. A scramble control (ctrl shRNA) and two shRNA constructs that specifically target the human OBSCN gene (obsc shRNA-1 and obsc shRNA-2) were commercially obtained (OriGene Technologies). The sequences of the shRNA (from 5′ to 3’ on the sense strand) are as follows, obsc shRNA-1: AGAGGCAGGAGCCAGTGCCACACTGAGCT and obsc shRNA-2: CTTGAGGATGCTGGAACTGTCAGTTTCCA. shRNA oligonucleotides were cloned into the pGFP-V-RS plasmid vector that incorporates a puromycin resistance marker (OriGene Technologies). Cell transfection was performed using Lipofectamine 3000 (Invitrogen). Stably transfected cells were selected by adding puromycin (Gibco; 500 ng/ml) to the medium three days after transfection. Stable clones expressing obsc shRNA-1, shRNA-2 or ctrl-shRNA were isolated and propagated in complete medium in the presence of puromycin. All experiments were performed with pooled clones of each stable line.

Stable scramble control and obscurin knockdown Panc5.04 pancreatic cancer cell lines were also generated with shRNA lentivirus technology. The lentivirus shRNA target sequences are (from 5′ to 3’ on the sense strand): scramble control: GCACTACCAGAGCTAACTCAGATAGTAC, obscurin shRNA-3: CGGAGGTGATGTGGTACAAAG, obscurin shRNA-4: GCCCAATTCGAGGCTATCATT (Fig. 1A). The shRNA sequences were cloned into pLKO.1 puro (Addgene, plasmid # 8453) lentivector with a puromycin antibiotic selection marker via BshT1 and EcoR1 restriction sites with standard molecular cloning techniques. The viruses were produced in HEK293T cells. Successfully transduced cells were selected with 20 μg/ml puromycin.

2.3. Antibodies

The antibodies used in this study are: RhoA (7F1.E5) mouse monoclonal antibody (Cytoskeleton, ARH04); Actin (C4) mouse monoclonal antibody (BD Transduction, 612656); HSP90 (C45G5) rabbit monoclonal antibody (Cell Signaling Technology, 4877); Phospho-Paxillin (Tyr118) rabbit polyclonal antibody (Cell Signaling Technology, 2541); Obscurin COOH-terminal rabbit polyclonal antibody or Obscurin NH_2-terminal mouse monoclonal antibody [9]; Obscurin Ig 58/59 rabbit polyclonal antibody [16]; Phospho-Myosin Light Chain 2 (Ser 19) rabbit monoclonal antibody (Cell Signaling Technology, 3671).

2.4. Western blots

Cells were lysed in radioimmunoprecipitation assay (RIPA, Thermo Scientific) buffer in the presence of protease inhibitors (Roche). Protein lysates of equal quantities, determined using the BCA assay kit (ThermoFisher), were separated using a 3–8% Tris-acetate SDS-PAGE gel or a 4–12% Bis-Tris gel (Bio-Rad) and transferred onto nitrocellulose membranes for subsequent blotting. For the obscurin western blots, membranes were blocked for 2–8 h either in 10% milk in Phosphate Buffered Saline (PBS) with 0.1% Tween-20 and 0.02%

Author Manuscript Author Manuscript Author Manuscript Author Manuscript

sodium azide or 5% milk in Tris Buffered Saline (TBS) with 0.1% Tween-20 before incubation with primary antibodies against obscurins, followed by the appropriate alkaline phosphatase (AP) or horseradish peroxidase (HRP) conjugated anti-mouse or anti-rabbit secondary antibodies (Jackson ImmunoResearch, 1:300). For the RhoA western blots, the membranes were blocked for 1 h in TBS containing 1% BSA and 0.1% Tween-20 before probing with the appropriate primary antibody followed by anti-mouse or anti-rabbit HRP-linked secondary antibodies (Cell Signaling, 1:2000). Immunoreactive bands were visualized with the Tropix chemiluminescence (Thermo Fisher) and the Pierce ECL Western Blotting Substrate (Thermo Fisher) or SignalFire ECL Reagent (Cell Signaling Technology) kits for the AP and HRP systems, respectively. Densitometric evaluation of immunoreactive bands was performed with ImageJ software.

2.5. Immunofluorescence

In most experiments, cells were fixed with 3.7% paraformaldehyde, permeabilized with 0.25% Triton X-100 in PBS and incubated in blocking buffer consisting of PBS with 10% normal goat serum (NGS) and 1% bovine serum albumin (BSA) for at least 1 h. For phospho-Myosin Light Chain (pMLC) staining, cells were fixed with 4% paraformaldehyde, permeabilized with 0.1% Triton X-100, and blocked in 5% NGS, 5% BSA and 0.2% Triton X-100 in PBS. Cells were then treated overnight at 4 °C with the indicated primary antibodies diluted in blocking buffer, followed by incubation with an appropriate secondary Alexa Fluor 488 or 568 goat anti-mouse or anti-rabbit secondary antibody (Invitrogen) at a 1:200 dilution in blocking buffer unless otherwise specified. The samples were washed thoroughly with PBS between each step. Slides were mounted with ProLong™ Gold Antifade reagent (Invitrogen) and imaged using either a LSM510 or LSM700 laser scanning confocal microscope with either a 40X or 63X objective lens. In pMLC experiments, specimens were imaged using a Nikon A1 confocal microscope with a 60X/1.4 N.A. oil immersion objective lens.

2.6. Immunohistochemistry

Human pancreatic cancer tumor microarray slides containing paraffin-embedded PDAC and matched normal adjacent tissue (US Biomax Inc) were evaluated for obscurin expression. Specimens included 3 biopsies of invasive ductal carcinoma (IDC) grade-1, 2 biopsies of IDC grade 1/2, 51 biopsies of IDC grade 2, 12 biopsies of IDC grade 2/3, and 7 biopsies of IDC grade 3 tumors. The tumor microarray was deparaffinized in xylene and rehydrated using ethanol washes. Antigen retrieval was performed using 10 mM sodium citrate buffer at 90°C followed by washes with cold water. Tissue sections were washed with TBS containing 0.025% Triton X-100, and blocked with TBS supplemented with 10% NGS and 1% BSA for at least 4 h prior to overnight incubation at 4°C with the rabbit polyclonal obscurin Ig 58/59 antibody diluted in TBS with 1% BSA. Slides were then washed with TBS containing 0.025% Triton X-100, and incubated with goat anti-rabbit Alexa Flour 488 secondary antibody. Following washes in TBS with 0.025% Triton X-100, the samples were mounted with ProLong™ Gold Antifade reagent, imaged using a LSM700 laser scanning confocal microscope with a 40x objective lens. The obtained fluorescent signals were independently quantified by two investigators using ImageJ by including the

Author Manuscript Author Manuscript Author Manuscript Author Manuscript

entirety of each tissue specimen; the PDAC values were normalized to those of the normal tissue for each matched tissue pair.

2.7. Microchannel migration assay

Polydimethylsiloxane (PDMS)-based microchannel devices were fabricated using photolithography and standard replica molding techniques as previously described [25,26]. Each device consists of a series of parallel microchannels of 200 μm in length, 10 μm in height and prescribed widths (3, 6, 10 or 20 μm), which are arrayed in a ladder-like configuration perpendicularly between a cell seeding and a chemoattractant channel [25,27]. All microchannels were coated with collagen type I (20 μg/ml). Cell migration was visualized and recorded via time-lapse live microscopy in an enclosed, humidified stage top incubator (Tokai Hit) maintained at 37 °C and 5% CO_2 using stage automation and a Nikon Inverted microscope. Images were taken at 10–20 min interval with a 10x Ph1 objective. FBS (10%) in medium containing 1% penicillin/streptomycin was used as chemoattractant. The spatial x and y positions of all non-dividing and viable cells that entered and migrated in the microchannels were tracked over time with the Manual Tracking plugin in ImageJ. Migration velocities were computed using a custom-written MATLAB code as previously described [25,27]. Cell morphological parameters, such as circularity and solidity, were also quantified using ImageJ [28]. In select experiments, cells were incubated in medium containing blebbistatin (2–10 μM, Sigma-Aldrich) or the vehicle control dimethyl sulfoxide (DMSO), prior to their seeding in the microchannel devices.

2.8. RhoA activity assays

RhoA activity was measured by RhoA Pulldown Activation Assay or confocal fluorescence-lifetime imaging microscopy (FLIM) using a Förster resonance energy transfer (FRET) RhoA2G sensor. RhoA Pulldown Activation Assay (Cytoskeleton) was performed according to the manufacturer's protocol with ctrl shRNA and obsc-KD shRNA HPDE and Panc5.04 cells. In FLIM-FRET assays, ctrl shRNA, shRNA-3 and shRNA-4 Panc5.04 cells were transduced with pLentiRhoA2G sensor and imaged using a Zeiss LSM 780 microscope and a PicoQuant FLIM system as previously described [29,30]. Cells migrating on collagen I-coated 2D surfaces were imaged at a single scan of a 1024 × 1024-pixel window, and data were quantified using SymPhoTime 64 (PicoQuant) software [29,30].

2.9. Microtubule (MT) dynamics quantified using microtubule associated protein EB family member 1 (EB1) assay

Cells with control or obscurin shRNA were transfected with EB1-GFP (Addgene) using Lipofectamine 3000 (Invitrogen) according to the manufacturer's protocol. 48 h after transfection, cells were re-plated on a collagen type I-coated glass surface and allowed to adhere overnight. EB1-GFP-expressing cells with control or obscurin shRNA-3 and -4 were imaged every 3 s for 6 min using a Nikon A1 confocal microscope (Nikon, Tokyo, Japan) with a 60X/1.4 N.A. oil immersion objective lens. In select experiments, cells were treated with (S)-4′-nitro-blebbistatin (Cayman) (0.5–1 μM) or vehicle control (DMSO) for at least 1 h prior to confocal imaging. Cells with control or obscurin shRNA-1 and -2 were imaged with Zeiss LSM 700 laser scanning confocal microscope with a 63X/1.4 NA oil-immersion objective lens every 3.08 s for 6.16 min. At least 10 different EB1-comets in each cell were

Author Manuscript Author Manuscript Author Manuscript Author Manuscript

analyzed and imaged. Life history plots and kymographs of EB1-GFP comets in each cell were generated and used to quantify MT growth rates via ImageJ as previously described [24,25].

2.10. Focal adhesion (FA) measurements with total internal reflectance fluorescence (TIRF) microscopy or confocal microscopy

5×10^4 cells were seeded on collagen type I-coated glass coverslips or glass bottom dishes and allowed to adhere for 24 h. Cells were fixed and stained as previously described [24,31,32] using a primary rabbit polyclonal antibody against phosphorylated-paxillin (Tyr118) (pY-paxillin) (Cell Signaling Technology, 1:50) and goat anti-rabbit Alexa Fluor 568 secondary antibody (Invitrogen, 1:2000). FAs were visualized and quantified by TIRF microscopy using a 3i Mariana inverted microscope (Intelligent Imaging Innovation) with a 100X/1.45 N.A. oil immersion objective lens and Slidebook 8.0 software [24]. In brief, after adjusting for background staining, images were rendered binary, and the particle analyzer tool in ImageJ was used to enumerate pY-paxillin-positive punctate areas greater than 0.1 μm^2. The total FA area, the number of FA per cell area and the area of FA per cell were then calculated.

Panc5.04 cells with control shRNA or obscurin shRNA-3 and -4 were seeded on collagen type I-coated glass bottom dishes and allowed to adhere for 20–24 h. In select experiments involving drug treatments, adhered cells were incubated with the prescribed pharmacological agents for 4 h prior to fixation and staining with pY-paxillin. Cells were imaged using a Nikon A1 confocal microscope (Nikon, Tokyo, Japan) using a 60X/1.4 N.A. oil immersion objective lens. Once the basal plane was identified and background signal was subtracted, FAs were quantified using custom macros within the General Analysis command of NIS Elements (Nikon). Adhesions with a max ferret value less than 0.1 μm and greater than 10 μm were excluded.

2.11. Actin dynamics quantified with fluorescence recovery after photobleaching (FRAP)

Cells were transfected with either Lifeact-RFP (Addgene) or pCT-Actin-GFP (System Biosciences) using Lipofectamine 3000 (Invitrogen) according to the manufacturer's protocol. 48 h after transfection, cells were replated on a glass slide coated with collagen type I and allowed to adhere overnight and form a confluent monolayer. Lifeact-RFP-expressing cells were imaged with a Zeiss LSM 700 laser scanning confocal microscope with a 63X/1.4 NA oil-immersion objective lens. Circular regions of interest of 4 μm in diameter were selected at cell-cell borders, and were photobleached with 568-nm laser at 100% power. Images were captured every 1.04 s before and after photobleaching. pCT-Actin-GFP-expressing cells were imaged with Nikon A1 confocal microscope (Nikon, Tokyo, Japan) using a 60X/1.4 N.A. oil immersion objective lens and were photobleached with 488-nm laser at 100% power. In select experiments, cells were treated with Y27632 (10 μM) or vehicle control (medium) for at least 1 h prior to confocal imaging. The FRAP time-lapse videos were analyzed with ImageJ as previously described [16,24,26].

Author Manuscript Author Manuscript Author Manuscript Author Manuscript

2.12. Subcutaneous implantation model

The subcutaneous model was adopted to evaluate the contribution of giant obscurins to *in vivo* tumor growth. All animal work was approved and performed in compliance with the Institutional Animal Care and Use Committee (IACUC) at the Johns Hopkins University. Eight-week old NSG mice were subcutaneously injected into both flanks with either ctrl-shRNA or obsc-shRNA HPDE or Panc5.04 cells (4×10^6 cells/ml in 50% matrigel) [24]. Tumor size was measured with calipers in a blinded manner, and the corresponding volume was calculated using the ellipsoid shape model. Mice were euthanized by CO_2 inhalation according to the IACUC protocol 83 days after injection. Tumors were harvested, weighed and fixed in 10% buffered formalin phosphate.

2.13. Hemispleen injection model

To investigate the role of obscurins in PDAC metastasis *in vivo*, we adopted the well-established preclinical murine model of hepatic metastasis following hemispleen injection [24,33]. All animal work was performed in accordance with IACUC protocols at the Johns Hopkins University. Human Panc5.04 cells were selected as the model PDAC cell line for *in vivo* experiments because they possess high expression levels of giant obscurins and moderate tumorigenic potential *in vivo* [34]. In brief, control shRNA, obscurin shRNA-3 or shRNA-4 Panc5.04 cells were dissociated, resuspended into a final concentration of 2×10^7 cell/ml in anti-clumping buffer diluted 1:1000 in Hanks' balanced salt solution (Gibco) and maintained on ice. 6–8 weeks old female NOD-SCIDγ (NSG) mice were purchased from Johns Hopkins Research Animal Resources (Baltimore, MD, USA) and maintained in accordance with IACUC guidelines. Mice were prepped under anesthesia induced by isoflurane inhalation before a left subcostal incision was made to locate the spleen. The spleen was eviscerated, clipped and divided in half. 100 μl of cell suspension (containing 2×10^6 Panc5.04 pancreatic cancer cells) was injected to one half of the spleen, followed by a flush with 150 μl of ice-cold PBS, while the other half was placed back into the peritoneum to avoid contamination. Pancreatic cancer cells were allowed to flow into the liver via the splenic vessels for 2 min, after which the injected half of the spleen and splenic vessels were clipped and removed, followed by suturing. 70 days post injection, all mice were sacrificed by CO_2 inhalation. Livers were harvested postmortem during necropsy and examined macroscopically for quantifying the number of visible macrometastases by two independent investigators in a blinded manner, and then flash-frozen by immersion in liquid nitrogen for subsequent qPCR analysis of human long interspersed nuclear element-1 (*hLINE-1*) to quantify metastatic tumor burden.

In separate experiments aimed to evaluate the role of giant obscurins in mouse survival using the hemispleen injection technique, mice were euthanized by CO_2 inhalation when they displayed morbid characteristics, and their survival times were recorded. All mice were monitored regularly according to IACUC guidelines.

2.14. DNA extraction and hLINE-1 quantification

DNA was extracted from frozen liver specimens, as described in Refs. [16,35–37], using the DNeasy Blood and tissue kit (Qiagen) according to the manufacturer's recommendations. Specifically, three pieces (<25 mg per piece) were collected from each harvested liver

Author Manuscript Author Manuscript Author Manuscript Author Manuscript

in a sterile biological safety cabinet to minimize human DNA contamination, weighed and recorded. Tissue samples were lysed overnight at 56 °C. Following the purification steps outlined in the manufacturer's protocol, DNA samples were eluted with 200 μl of DNA-RNA free water. Quantification of *hLINE-1* levels, which serve as a proxy of the amount of human DNA present in mouse livers, was performed with qPCR as reported in Refs. [16,35–37] with some modifications. Briefly, qPCR was performed in 20 μl volume of DNA samples with the following components: 10 μl iTaq Universal SYBR Green Supermix (Bio-Rad), 1.5 μl each of 10 μM forward (5′-TCACTCAAAGCCGCTCAACTAC-3′) and reverse (5′-TCTGCCTTC ATTTCGTTATGTACC-3′) primers, 4.5 μl purified DNA and 2.5 μl water. The reaction was run on an iCycler/iQ5 (Bio-Rad) with the following cycling conditions: (94 °C, 2 min) × 1, (94 °C, 10 s; 67 °C, 15 s; 70 °C, 15 s) × 3, (94 °C, 10 s; 64 °C, 15 s; 70 °C, 15 s) × 3, (94 °C, 10 s; 61 °C, 15 s; 70 °C, 15 s) × 3, and (94 °C, 10 s, 59 °C, 15 s; 70 °C, 15 s) × 35. The threshold cycle number was calculated using the Bio-Rad iQ5 software. Serial dilutions of human DNA extracted from Panc5.04 cells using the DNeasy Blood and tissue kit (Qiagen) were included in each measurement to serve as standards.

2.15. Statistical analysis

Data represent the mean ± S.E.M. from 3 independent experiments unless otherwise stated. The D'Agostino-Pearson omnibus normality test was used to determine whether data are normally distributed. Data sets with Gaussian distributions were compared using Student's t-test (two-tailed) or one-way ANOVA followed by Tukey's post-hoc test wherever appropriate. For comparing non-Gaussian distributions, the nonparametric Mann-Whitney or Kruskal-Wallis test was used for comparisons between two or more groups, respectively. For comparisons between multiple groups with two independent variables, two-way ANOVA was used followed by Šídák multiple comparisons test. Statistical significance was defined as $p < 0.05$. Calculations were performed using GraphPad Prism 7, 8 or 9 (GraphPad Software).

3. Results

Reduced expression of giant obscurins in PDAC compared to normal pancreatic epithelial tissues.

While the *OBSCN* gene has been identified as a frequently mutated gene in PDACs [21] (Supplementary Fig. S1A and B), the protein expression levels of obscurin in normal versus PDAC tissues have yet to be characterized. To this end, we evaluated the expression profile of obscurins using tissue microarrays containing human biopsies from 75 PDACs of grade 1–3 and matched adjacent normal tissue. Specimens were stained with an antibody specific to the Ig58/59 region of giant obscurins A and B (Fig. 1A) and imaged using confocal microscopy. Obsurins were abundantly expressed in normal samples where they exhibited a relatively uniform distribution, but were markedly reduced in adjacent tumor biopsies, as determined by quantification of the obtained fluorescent signals, with residual obscurins detected at the cell membrane and/or in puncta (Fig. 1B–D). Consistent with these findings, examination of the expression profile of *OBSCN*, using the TNM web tool (https://www.tnmplot.com/) that uses publicly available transcriptomic expression data and

Author Manuscript Author Manuscript Author Manuscript Author Manuscript

provides information about the differential expression of genes between normal and tumor biopsies, indicated significantly reduced expression of *OBSCN* in PDACs versus normal samples (Supplementary Fig. S1C).

To investigate the functional consequences of reduced expression of *OBSCN* in pancreatic cancer, we next screened normal and cancer pancreatic epithelial cells for obscurin expression via immunoblotting (Fig. 1E) to identify candidate cell lines for depleting obscurins. We focused on giant obscurins in view of their function as tumor suppressors in breast epithelial cells [15,16]. Normal-like, non-tumorigenic HPDE cells and Panc5.04 pancreatic cancer cells consistently expressed high levels of giant obscurins (Fig. 1E and Supplementary Fig. S1D and E); of note, the kinase-bearing obscurin-B is the most prevalent isoform in all pancreatic cell lines tested. Immunostaining further confirmed the expression of obscurins in HPDE and Panc5.04 cells (Supplementary Fig. S1F and H). Obscurins concentrate in perinuclear/cytoplasmic puncta and the nucleus in HPDE cells grown in the absence of FBS (Supplementary Fig. S1G). We reasoned that this may be a result of the lack of serum in the culture medium. Indeed, upon treatment with 10% FBS for 24 h, obscurins translocated to cell-cell junctions in HPDE cells (Supplementary Fig. S1G), which resembles the localization profile of obscurins in Panc5.04 and SW1990 pancreatic cancer cells cultured in serum-containing medium (Supplementary Fig. S1H and I). Of note, the nuclear and cell-cell junction localization patterns of obscurins in pancreatic cells are consistent with those observed in breast epithelial cells [15].

Knockdown of giant obscurins in human pancreatic ductal epithelial HPDE cells promotes migration along with a protrusive phenotype via cytoskeletal remodeling.

To investigate the impact of decreased levels of obscurins observed in PDAC relative to adjacent normal tissue, we generated stable obscurin-knockdown HPDE cells expressing either shRNA-1 targeting Ig10 or shRNA-2 targeting Ig58 (Fig. 1A) as well as control HPDE cells expressing a scramble shRNA plasmid (ctrl shRNA). Western blot analysis validated the successful knockdown of both obscurins A and B in HPDE cells (Fig. 2A) ranging between 60 and 80% (Supplementary Fig. S2A). Evaluation of obscurin-depleted HPDE cells indicated that they were more protrusive and elongated than scramble control cells as evidenced by their lower solidity and circularity, respectively, and migrated faster inside 10 μm-wide microchannels (Fig. 2B–E and Supplementary Fig. S2B–D).

Earlier work has shown that the RhoGEF motif of obscurins specifically binds and activates RhoA [38]. In fact, the activation of RhoA by the RhoGEF domain is conserved for the nematode homolog of obscurin, called UNC-89 [39]. We therefore performed RhoA pull-down assays to quantify RhoA activity in obscurin-expressing and obscurin-depleted HPDE cells. Knockdown of giant obscurins significantly diminished the levels of active RhoA by 40–60% as compared to control shRNA (Fig. 3A and Supplementary Fig. S3A).

It is well established that RhoA regulates the cytoskeletal and adhesion dynamics in migrating cells [29,40]. Downregulation of RhoA activity alters microtubule (MT) dynamics and decreases focal adhesion (FA) size and stress fiber formation. Given that the formation of stable MTs is induced by RhoA [41], and downregulation of RhoA activity is associated with increased MT dynamics [42], we next quantified MT growth in control and obscurin-

Author Manuscript Author Manuscript Author Manuscript Author Manuscript

depleted HPDE cells via live-cell confocal imaging of EB1-GFP, a protein which binds to the plus end of growing MT [25,43]. Cells transfected with EB1-GFP were imaged over 6 min, and growing MT comets were tracked over time to calculate the rate of MT growth (Fig. 3B). Obscurin knockdown promoted significantly faster MT growth rates in HPDE cells (Fig. 3C and Supplementary Fig. S3B), which is consistent with the notion that downregulation of RhoA activity mediated by obscurin depletion results in increased MT dynamics.

To assess the role of giant obscurins in FA size and density, FAs were visualized and quantified via TIRF imaging of HPDE cells immunostained for phospho-tyrosine (pY)-paxillin [24], which is a signaling adapter protein found at FAs of non-muscle cells. While FAs were found to be concentrated primarily at the cell periphery of control HPDE cells, they were distributed throughout the cell surface of obscurin knockdown cells (Fig. 3D). Importantly, knockdown of obscurins decreased FA density and size (Fig. 3E and Supplementary Fig. S3C).

Using FRAP, we also quantified the actin dynamics at the cell-cell junctions of Lifeact-RFP-transfected control and obscurin-KD HPDE cell monolayers. Because obscurin localizes at the HPDE cell-cell junctions only in the presence of FBS (Supplementary Fig. S1E and F), these assays were performed in medium supplemented with 10% FBS. Obscurin-depleted relative to control HPDE cells displayed higher Lifeact-RFP mobile fraction, while no significant difference was observed for the recovery half-life (Fig. 3F, Supplementary Fig. S3D). These findings suggest that obscurin silencing increases actin dynamics. As a control, we performed these measurements in serum-free medium where obscurins fail to localize at cell-cell junctions, and found no differences in either the mobile fraction or half-life of Lifeact-RFP recovery for control and obscurin knockdown cells (Supplementary Fig. S3E and F). Taken together, depletion of obscurins downregulates RhoA activity and alters cytoskeletal dynamics.

Although knockdown of giant obscurins in normal HPDE cells promoted cell locomotion via cytoskeletal remodeling, it failed to induce primary tumor formation in a subcutaneous implantation model. These findings suggest that depletion of giant obscurins is not sufficient to induce tumorigenesis, which is consistent with their role as tumor suppressors. Thus, we next tested the effects of obscurin knockdown on pancreatic cancer cell function *in vitro* and *in vivo*. Panc5.04, which is a tumorigenic cell line derived from a stage IIB primary pancreatic tumor, was chosen as a model cell system for subsequent studies.

Knockdown of giant obscurins in Panc5.04 pancreatic cancer cells promotes faster migration *in vitro* via regulation of cytoskeletal dynamics and increases tumor growth *in vivo*.

Obscurin-knockdown Panc5.04 pancreatic cancer cells were generated (Fig. 4A and Supplementary Fig. S4A) using three different shRNA sequences (Fig. 1A) by either transfecting cells with control or obscurin shRNA-2 followed by clonal selection or using the lentiviral technology for shRNA-3 and -4 targeting Ig11 and Ig68, respectively. Consistent with the data acquired using non-cancerous HPDE cells, obscurin depleted Panc5.04 cells exhibited markedly reduced levels of active RhoA as quantified by RhoA

Author Manuscript Author Manuscript Author Manuscript Author Manuscript

pulldown activation assays (Supplementary Fig. S4B) or by FLIM-FRET as measured by the increased donor fluorescence lifetimes (Fig. 4B). In line with the reduced RhoA activity, its downstream effector pMLC levels were also decreased (Fig. 4C). These biochemical changes were accompanied by a more elongated cell morphology and a more migratory phenotype in obscurin knockdown compared to scramble control cells as evidenced by their lower circularity (Fig. 4D), smaller FAs (Fig. 4E) and faster motility (Fig. 4F and Supplementary Fig. S4C and D).

To demonstrate the critical role of RhoA activity and the downstream myosin II-dependent contractility in the morphological and phenotypic alterations induced in obscurin-knockdown cells, we first examined the dose-dependent effect of blebbistatin (2–10 μM), which inhibits actomyosin contractility, on cell migration. Scramble control Panc5.04 cells, which possess high RhoA activity, displayed a biphasic response to increasing blebbistatin concentrations (Supplementary Fig. S4E). Specifically, low (2 μM) and high (10 μM) concentrations of blebbistatin did not alter the velocity of scramble control Panc5.04 cells relative to vehicle control, whereas 5 μM of blebbistatin significantly increased cell motility (Supplementary Fig. S4E). On the other hand, the velocity of obscurin-knockdown cells, which display significantly lower RhoA activity, was insensitive to low or medium concentrations (2–5 μM) of blebbistatin but was significantly reduced after treatment with 10 μM blebbistatin (Supplementary Fig. S4E). Interestingly, treatment of scramble control and obscurin-knockdown Panc5.04 cells with 5 μM blebbistatin abrogated the differences detected between these two cell types in cell morphology (Fig. 4D), FA size (Fig. 4E), and migration velocity (Fig. 4F). Cumulatively, these data illustrate that suppression of RhoA activity induced by obscurin depletion or partial inhibition of the downstream myosin II-dependent contractility promotes faster motility.

In accord with the results obtained using non-tumorigenic obscurin-deficient HPDE cells, obscurin-knockdown Panc5.04 cells also exhibited faster MT growth rate (Fig. 4G) and actin dynamics (Fig. 4H and Supplementary Fig. S4F), thereby demonstrating the role of giant obscurins in cytoskeletal reorganization. Importantly, treatment of ctrl shRNA Panc5.04 cells with an intermediate concentration of (S)-4′-nitro-blebbistatin (0.5 μM) increased MT growth rate to levels of untreated obscurin-knockdown cells (Supplementary Fig. S4G). Of note, this concentration had a modest effect on the MT dynamics of obscurin-knockdown cells relative to vehicle controls. Use of the RhoA/ROCK inhibitor Y27632 reveals the involvement of this pathway, which is regulated by obscurin, in the modulation of actin dynamics as evidenced by FRAP measurements (Supplementary Fig. S4H). Taken together, these data confirm and extend our observations with normal HPDE cells showing that obscurin depletion alters cell morphology and promotes faster migration via downregulation of RhoA activity, which in turn modulates cytoskeletal remodeling and dynamics.

Obscurin silencing also accelerated tumor growth in a subcutaneous implantation model (Fig. 4I–K). Although both scramble control and obscurin-shRNA-2 Panc5.04 cells generated palpable tumors of equivalent volume within 30 days post injection, tumor volume increased at a higher rate for obscurin knockdown specimens at about 70 days post implantation (Fig. 4I). These data were confirmed by measuring the volume and weight

Author Manuscript Author Manuscript Author Manuscript Author Manuscript

of the harvested tumors at necropsy (Fig. 4J and K and Supplementary Fig. S4I), thereby suggesting that obscurin knockdown potentiates tumorigenicity *in vivo*.

Silencing of giant obscurins in Panc5.04 pancreatic cancer cells shortens survival by exacerbating metastasis.

To evaluate whether the faster migratory potential of obscurin knockdown pancreatic cancer cells observed *in vitro* coupled with their elevated tumor growth *in vivo* alter survival and metastasis, we used the preclinical murine hepatic metastasis model via hemispleen injection to inoculate scramble control and obscurin shRNA-3 or shRNA-4 Panc5.04 cells [24]. Mice that survived the surgical procedure were monitored over time and euthanized when they exhibited morbid symptoms (Fig. 5A). Analysis of the Kaplan-Meier survival curves reveals that obscurin silencing significantly shortened mouse survival (Fig. 5A). Specifically, the median survival time of mice injected with control shRNA-expressing Panc5.04 cells was 115 days as compared to 83 and 88 days for obscurin shRNA-3- and shRNA-4-expressing cells, respectively. Moreover, post mortem dissection and visual inspection of the livers showed that mice injected with obscurin shRNA-4 Panc5.04 cells developed significantly more liver macrometastases relative to control shRNA (Supplementary Fig. S5A and B). While there was no statistically significant difference in the average number of visible liver macrometastases between mice injected with control shRNA- versus obsc shRNA-3-expressing Panc5.04 cells, this is due to the larger liver tumors generated by the obscurin-knockdown cells (Supplementary Fig. S5A–B).

While the previous set of experiments demonstrates that silencing of giant obscurins negatively impacts mouse survival, its effect on metastasis is confounded by the marked differences in the euthanasia time points. To accurately quantify and compare the metastatic potentials of scramble control and obscurin-knockdown Panc5.04 cells, we repeated the hemispleen injection experiment with the modification of sacrificing all mice concurrently 70 days post injection (Fig. 5B), which corresponded to the time point at which the first mouse/mice fulfilled the criteria of euthanasia. Consistent with the survival analysis data, obscurin shRNA-4-, but not shRNA-3-, expressing Panc5.04 cells generated a significantly higher number of liver macrometastases relative to control shRNA (Fig. 5B’). In light of gross anatomical images of representative livers showing the formation of larger albeit fewer macrometastatic tumors in mice injected with shRNA-3-expressing cells, we quantified metastatic tumor burden by measuring the amount of human DNA present via qPCR using primers specific for *hLINE*. Our analysis reveals that livers harvested from mice following splenic injection with obscurin shRNA-3- or obscurin shRNA-4-expressing Panc5.04 cells contained significantly higher amount of human DNA relative to control shRNA (Fig. 5B’’), which is in line with the gross anatomy photographs (Fig. 5C). Taken together, these highlight the pivotal role of giant obscurins in accelerating pancreatic cancer growth and metastasis *in vivo*, thereby shortening survival.

4. Discussion

Cancer cells acquire multiple and successive genetic alterations, which ultimately result in the deregulation of major signaling pathways and the generation of non-canonical feedback

Author Manuscript Author Manuscript Author Manuscript Author Manuscript

loops that together promote uncontrolled cell proliferation, anoikis escape, migration and invasion. *OBSCN*, originally identified as a structural and signaling mediator of the cytoskeleton in muscle cells [5], has recently emerged as a potent tumor suppressor [16] that is heavily mutated across different types of cancer [44]. However, functional studies interrogating *OBSCN*'s role in normal non-muscle cells and the impact of its loss are lacking with the exception of breast epithelium [15,16].

Pancreatic cancer is one of the deadliest cancers currently accounting for ~3% of all cancers in the US and ~7% of all cancer-related deaths, with an average lifetime risk of ~1 in 64. These dreary statistics are further highlighted by a recent projection indicating that the number of deaths due to pancreatic cancer will exceed those of colorectal cancer before 2030, rendering pancreatic cancer as the second leading cause of cancer-related deaths in the US [45]. The lack of effective targeted treatment modalities and the paucity of validated molecular biomarkers providing prognostic information about the progression and severity of the disease are key factors contributing to the poor survival of affected patients [46]. Importantly, the presence of mutations in *OBSCN* is predicted to be damaging in pancreatic cancer [21]. In agreement with this, electrospray mass spectrometry demonstrated reduced levels of *OBSCN* peptides in the serum of stage IIb PDAC patients compared to control subjects [47].

In view of these observations and given the mutational prevalence of *OBSCN* in pancreatic cancer [21], we evaluated the expression profile of *OBSCN* in microarrays of pancreatic tumor biopsies and adjacent normal tissue. We found the expression levels of *OBSCN* to be drastically reduced in tumor biopsies compared to normal tissue, implicating *OBSCN* loss in pancreatic cancer pathogenicity. This notion was corroborated by our functional studies investigating the consequences of *OBSCN*'s loss in pancreatic cells. In line with the purported role of *OBSCN* as tumor suppressor [16,44], our findings show that silencing of giant obscurins in pancreatic cells potentiates tumor growth and metastasis via cytoskeletal remodeling mediated, at least in part, through alterations in RhoA signaling.

Giant obscurins contain a tandem array of signaling motifs including a RhoGEF motif that has been shown to specifically bind and activate RhoA [38]. In line with our previous work in breast epithelial cells [32, 48], knockdown of giant obscurins in pancreatic cells suppresses RhoA activity. Consistent with the decreased RhoA activity [40], obscurin-depleted pancreatic cells display a more elongated and protrusive phenotype, characteristic of malignant transformation.

RhoA and its downstream effectors are key regulators of adhesion, MT and actin organization [49,50]. Indeed, downregulation of RhoA activity via obscurin silencing or inhibition of myosin II activity with low concentrations of blebbistatin promotes MT growth and reduces FA density and size, thereby promoting faster migration. These findings are in accord with prior work showing the interplay between RhoA-dependent signaling and MTs as well as the role of MT growth in focal adhesion disassembly [49,51]. Our data also reveal the "goldilocks" or biphasic effect of myosin II inhibition on the migration velocity of obscurin-expressing cells where intermediate concentrations of blebbistatin (5 μM) facilitate motility, whereas low (2 μM) or high (10 μM) doses have little effect.

Author Manuscript Author Manuscript Author Manuscript Author Manuscript

Importantly, the average velocity of obscurin-expressing cells treated with an intermediate blebbistatin concentration is similar to that of untreated obscurin-knockdown cells, which exhibit reduced RhoA activity and pMLC levels. However, obscurin-depleted cells move slower upon treatment with a high dose (10 μM) of blebbistatin. Taken together, these findings are in concert with the notion that optimal levels of contractility are required for efficient cell locomotion as either too high or too low contractility supports a rather immotile or slowly moving cell phenotype. In addition to regulating focal adhesion assembly/disassembly and MT growth, giant obscurins alter actin dynamics via a RhoA/ROCK-dependent pathway. Specifically, obscurin depletion or ROCK inhibition in obscurin-expressing cells increases the mobile fraction of actin. A possible mechanism underlying this phenomenon may involve the actin-severing protein cofilin, which is a ROCK target [48] that displays increased activity in response to reduced phosphorylation. Consistent with this notion, inhibition of the RhoA/ROCK pathway via obscurin knockdown enhances cofilin activity [48], which in turn results in enhanced actin filament turnover, as evidenced by the increased mobile fraction of actin.

Because cell migration is critical to the dissemination of cancerous cells from a primary tumor to metastatic sites in the body, we examined the contributions of obscurins to pancreatic cancer progression and metastasis *in vivo* using the well-established preclinical model of pancreatic cancer metastasis to the liver via the hemispleen injection technique. NSG mice injected with obscurin-depleted Panc5.04 pancreatic cancer cells possessed a markedly higher tumor burden along with a shorter survival time than scramble controls. The enhanced metastatic capacity of obscurin-knockdown pancreatic cancer cells may be attributed not only to their higher migratory potential observed *in vitro* but also their elevated proliferation detected in an *in vivo* subcutaneous model. It is noteworthy that silencing of giant obscurins in normal, non-tumorigenic HPDE pancreatic epithelial cells was not able to induce *de novo* tumorigenesis after subcutaneous implantation. These data are consistent with the role of giant obscurins as tumor suppressors in pancreatic cancer not being sufficient to induce tumor formation, as carcinogenesis requires both the mutation of a proto-oncogene and the loss of function of a tumor suppressor gene [52].

In conclusion, we herein demonstrate that obscurins are abundantly expressed in normal pancreatic tissue biopsies but markedly reduced in adjacent tumor biopsies. Loss of giant obscurins from pancreatic epithelial or pancreatic cancer cells downregulates RhoA activity, which induces cytoskeletal remodeling by promoting MT growth and faster actin dynamics, and suppressing FAs, thereby facilitating cell migration *in vitro*. Accordingly, RhoA activity was found to be progressively decreased from normal pancreatic tissue to pancreatic intraepithelial neoplasias to advanced PDAC in mutant $KRas^{G12D/+}$ and $KRas^{G12D/+}/p53^{R172H/+}$ pancreatic cancer mouse models [53]. We therefore postulate that *OBSCN* loss from pancreatic cells leads to major cytoskeletal alterations, at least in part via deregulation of the RhoA/ROCK/myosin II axis, resulting in enhanced motility *in vitro* and increased proliferative capacity *in vivo*, which ultimately potentiate metastasis. The advent of CRISPR technology opens new possibilities in precision medicine. As such, our future studies will be directed at examining whether (re)activation of *OBSCN* expression in metastatic tumors would suppress migration/invasion *in vitro* and metastasis *in vivo*.

Author Manuscript Author Manuscript Author Manuscript Author Manuscript

Supplementary Material

Refer to Web version on PubMed Central for supplementary material.

Acknowledgments

This line of research was supported by the National Institutes of Health through grants R01-CA286186 (KK), R01-CA183804 (AKK, KK), R01 CA169702–06 (LZ), R01 CA197296–06 (LZ) and Sidney Kimmel Comprehensive Cancer Center Grant P30 CA006973 (LZ).

Data availability

All data needed to evaluate the conclusions in the paper are present in the paper and/or the Supplementary Materials.

References

[1]. Kamisawa T, Wood LD, Itoi T, Takaori K, Pancreatic cancer, Lancet 388 (2016) 73–85. [PubMed: 26830752]

[2]. Hruban RH, Maitra A, Goggins M, Update on pancreatic intraepithelial neoplasia, Int. J. Clin. Exp. Pathol. 1 (2008) 306–316. [PubMed: 18787611]

[3]. Collisson EA, Bailey P, Chang DK, Biankin AV, Molecular subtypes of pancreatic cancer, Nat. Rev. Gastroenterol. Hepatol. 16 (2019) 207–220. [PubMed: 30718832]

[4]. Kleeff J, Korc M, Apte M, La Vecchia C, Johnson CD, Biankin AV, Neale RE, Tempero M, Tuveson DA, Hruban RH, Neoptolemos JP, Pancreatic cancer, Nat. Rev. Dis. Primers 2 (2016) 16022. [PubMed: 27158978]

[5]. Russell MW, Raeker MO, Korytkowski KA, Sonneman KJ, Identification, tissue expression and chromosomal localization of human Obscurin-MLCK, a member of the titin and Dbl families of myosin light chain kinases, Gene 282 (2002) 237–246. [PubMed: 11814696]

[6]. Bang ML, Centner T, Fornoff F, Geach AJ, Gotthardt M, McNabb M, Witt CC, Labeit D, Gregorio CC, Granzier H, Labeit S, The complete gene sequence of titin, expression of an unusual approximately 700-kDa titin isoform, and its interaction with obscurin identify a novel Z-line to I-band linking system, Circ. Res. 89 (2001) 1065–1072. [PubMed: 11717165]

[7]. Young P, Ehler E, Gautel M, Obscurin, a giant sarcomeric Rho guanine nucleotide exchange factor protein involved in sarcomere assembly, J. Cell Biol. 154 (2001) 123–136. [PubMed: 11448995]

[8]. Fukuzawa A, Idowu S, Gautel M, Complete human gene structure of obscurin: implications for isoform generation by differential splicing, J. Muscle Res. Cell Motil. 26 (2005) 427–434. [PubMed: 16625316]

[9]. Ackermann MA, Shriver M, Perry NA, Hu LY, Kontrogianni-Konstantopoulos A, Obscurins: Goliaths and Davids take over non-muscle tissues, PLoS One 9 (2014), e88162. [PubMed: 24516603]

[10]. Wang L, Geist J, Grogan A, Hu LR, Kontrogianni-Konstantopoulos A, Thick filament protein network, functions, and disease association, Comp. Physiol. 8 (2018) 631–709.

[11]. Perry NA, Ackermann MA, Shriver M, Hu LY, Kontrogianni-Konstantopoulos A, Obscurins: unassuming giants enter the spotlight, IUBMB Life 65 (2013) 479–486. [PubMed: 23512348]

[12]. Sjoblom T, Jones S, Wood LD, Parsons DW, Lin J, Barber TD, Mandelker D, Leary RJ, Ptak J, Silliman N, Szabo S, Buckhaults P, Farrell C, Meeh P, Markowitz SD, Willis J, Dawson D, Willson JK, Gazdar AF, Hartigan J, Wu L, Liu C, Parmigiani G, Park BH, Bachman KE, Papadopoulos N, Vogelstein B, Kinzler KW, Velculescu VE, The consensus coding sequences of human breast and colorectal cancers, Science 314 (2006) 268–274. [PubMed: 16959974]

[13]. Balakrishnan A, Bleeker FE, Lamba S, Rodolfo M, Daniotti M, Scarpa A, van Tilborg AA, Leenstra S, Zanon C, Bardelli A, Novel somatic and germline mutations in cancer candidate genes in glioblastoma, melanoma, and pancreatic carcinoma, Cancer Res. 67 (2007) 3545–3550. [PubMed: 17440062]

Author Manuscript Author Manuscript Author Manuscript Author Manuscript

[14]. Price ND, Trent J, El-Naggar AK, Cogdell D, Taylor E, Hunt KK, Pollock RE, Hood L, Shmulevich I, Zhang W, Highly accurate two-gene classifier for differentiating gastrointestinal stromal tumors and leiomyosarcomas, Proc. Natl. Acad. Sci. U. S. A. 104 (2007) 3414–3419. [PubMed: 17360660]

[15]. Perry NA, Shriver M, Mameza MG, Grabias B, Balzer E, Kontrogianni-Konstantopoulos A, Loss of giant obscurins promotes breast epithelial cell survival through apoptotic resistance, Faseb. J. 26 (2012) 2764–2775. [PubMed: 22441987]

[16]. Shriver M, Stroka K, Vitolo M, Martin S, Huso DL, Konstantopoulos K, Kontrogianni-Konstantopoulos A, Loss of giant obscurins from breast epithelium promotes epithelial-to-mesenchymal transition, tumorigenicity and metastasis, Oncogene 34 (2015) 4248–4259. [PubMed: 25381817]

[17]. Rajendran BK, Deng CX, A comprehensive genomic meta-analysis identifies confirmatory role of OBSCN gene in breast tumorigenesis, Oncotarget 8 (2017) 102263–102276. [PubMed: 29254242]

[18]. Rajendran BK, Deng CX, Characterization of potential driver mutations involved in human breast cancer by computational approaches, Oncotarget 8 (2017) 50252–50272. [PubMed: 28477017]

[19]. Nalla AK, Williams TF, Collins CP, Rae DT, Trobridge GD, Lentiviral vector-mediated insertional mutagenesis screen identifies genes that influence androgen independent prostate cancer progression and predict clinical outcome, Mol. Carcinog. 55 (2016) 1761–1771. [PubMed: 26512949]

[20]. Babur O, Gonen M, Aksoy BA, Schultz N, Ciriello G, Sander C, Demir E, Systematic identification of cancer driving signaling pathways based on mutual exclusivity of genomic alterations, Genome Biol. 16 (2015) 45. [PubMed: 25887147]

[21]. Murphy SJ, Hart SN, Lima JF, Kipp BR, Klebig M, Winters JL, Szabo C, Zhang L, Eckloff BW, Petersen GM, Genetic alterations associated with progression from pancreatic intraepithelial neoplasia to invasive pancreatic tumor, Gastroenterology 145 (2013), e1091, 1098–1109. [PubMed: 23912084]

[22]. Jones S, Zhang X, Parsons DW, Lin JC, Leary RJ, Angenendt P, Mankoo P, Carter H, Kamiyama H, Jimeno A, Hong SM, Fu B, Lin MT, Calhoun ES, Kamiyama M, Walter K, Nikolskaya T, Nikolsky Y, Hartigan J, Smith DR, Hidalgo M, Leach SD, Klein AP, Jaffee EM, Goggins M, Maitra A, Iacobuzio-Donahue C, Eshleman JR, Kern SE, Hruban RH, Karchin R, Papadopoulos N, Parmigiani G, Vogelstein B, Velculescu VE, Kinzler KW, Core signaling pathways in human pancreatic cancers revealed by global genomic analyses, Science 321 (2008) 1801–1806. [PubMed: 18772397]

[23]. Dallas MR, Chen S-H, Streppel MM, Sharma S, Maitra A, Konstantopoulos K, Sialofucosylated podocalyxin is a functional E-and L-selectin ligand expressed by metastatic pancreatic cancer cells, Am. J. Physiol. Cell Physiol. 303 (2012) C616–C624. [PubMed: 22814396]

[24]. Wong BS, Shea DJ, Mistriotis P, Tuntithavornwat S, Law RA, Bieber JM, Zheng L, Konstantopoulos K, A direct podocalyxin-dynamin-2 interaction regulates cytoskeletal dynamics to promote migration and metastasis in pancreatic cancer cells, Cancer Res. 79 (2019) 2878–2891. [PubMed: 30975647]

[25]. Balzer EM, Tong Z, Paul CD, Hung WC, Stroka KM, Boggs AE, Martin SS, Konstantopoulos K, Physical confinement alters tumor cell adhesion and migration phenotypes, Faseb. J. 26 (2012) 4045–4056. [PubMed: 22707566]

[26]. Zhao R, Cui S, Ge Z, Zhang Y, Bera K, Zhu L, Sun SX, Konstantopoulos K, Hydraulic resistance induces cell phenotypic transition in confinement, Sci. Adv. 7 (2021), eabg4934. [PubMed: 33893091]

[27]. Tong Z, Balzer EM, Dallas MR, Hung WC, Stebe KJ, Konstantopoulos K, Chemotaxis of cell populations through confined spaces at single-cell resolution, PLoS One 7 (2012), e29211. [PubMed: 22279529]

[28]. Paul CD, Shea DJ, Mahoney MR, Chai A, Laney V, Hung WC, Konstantopoulos K, Interplay of the physical microenvironment, contact guidance, and intracellular signaling in cell decision making, Faseb. J. 30 (2016) 2161–2170. [PubMed: 26902610]

[29]. Mistriotis P, Wisniewski EO, Bera K, Keys J, Li Y, Tuntithavornwat S, Law RA, Perez N, Erdogmus E, Zhang Y, Zhao R, Sun SX, Kalab P, Lammerding J, Konstantopoulos K,

Author Manuscript Author Manuscript Author Manuscript Author Manuscript

Confinement hinders motility by inducing RhoA-mediated nuclear influx, volume expansion, and blebbing, J. Cell Biol. 218 (2019) 4093–4111. [PubMed: 31690619]

[30]. Yankaskas CL, Bera K, Stoletov K, Serra SA, Carrillo-Garcia J, Tuntithavornwat S, Mistriotis P, Lewis JD, Valverde MA, Konstantopoulos K, The fluid shear stress sensor TRPM7 regulates tumor cell intravasation, Sci. Adv. 7 (2021).

[31]. Hung W-C, Chen S-H, Paul CD, Stroka KM, Lo Y-C, Yang JT, Konstantopoulos K, Distinct signaling mechanisms regulate migration in unconfined versus confined spaces, J. Cell Biol. 202 (2013) 807–824. [PubMed: 23979717]

[32]. Stroka KM, Wong BS, Shriver M, Phillip JM, Wirtz D, Kontrogianni-Konstantopoulos A, Konstantopoulos K, Loss of giant obscurins alters breast epithelial cell mechanosensing of matrix stiffness, Oncotarget 5 (2016).

[33]. Foley K, Rucki AA, Xiao Q, Zhou D, Leubner A, Mo G, Kleponis J, Wu AA, Sharma R, Jiang Q, Anders RA, Iacobuzio-Donahue CA, Hajjar KA, Maitra A, Jaffee EM, Zheng L, Semaphorin 3D autocrine signaling mediates the metastatic role of annexin A2 in pancreatic cancer, Sci. Signal. 8 (2015) ra77. [PubMed: 26243191]

[34]. Zhong Y, Naito Y, Cope L, Naranjo-Suarez S, Saunders T, Hong S-M, Goggins MG, Herman JM, Wolfgang CL, Iacobuzio-Donahue CA, Functional p38 MAPK identified by biomarker profiling of pancreatic cancer restrains growth through JNK inhibition and correlates with improved survival, Clin. Cancer Res. 20 (2014) 6200–6211. [PubMed: 24963048]

[35]. Yankaskas CL, Thompson KN, Paul CD, Vitolo MI, Mistriotis P, Mahendra A, Bajpai VK, Shea DJ, Manto KM, Chai AC, Varadarajan N, Kontrogianni-Konstantopoulos A, Martin SS, Konstantopoulos K, A microfluidic assay for the quantification of the metastatic propensity of breast cancer specimens, Nat. Biomed. Eng. 3 (2019) 452–465. [PubMed: 31061459]

[36]. Wang P, Chen SH, Hung WC, Paul C, Zhu F, Guan PP, Huso DL, Kontrogianni-Konstantopoulos A, Konstantopoulos K, Fluid shear promotes chondrosarcoma cell invasion by activating matrix metalloproteinase 12 via IGF-2 and VEGF signaling pathways, Oncogene 34 (2015) 4558–4569. [PubMed: 25435370]

[37]. Dallas MR, Liu G, Chen WC, Thomas SN, Wirtz D, Huso DL, Konstantopoulos K, Divergent roles of CD44 and carcinoembryonic antigen in colon cancer metastasis, Faseb. J. 26 (2012) 2648–2656. [PubMed: 22415308]

[38]. Ford-Speelman DL, Roche JA, Bowman AL, Bloch RJ, The rho-guanine nucleotide exchange factor domain of obscurin activates rhoA signaling in skeletal muscle, Mol. Biol. Cell 20 (2009) 3905–3917. [PubMed: 19605563]

[39]. Qadota H, Blangy A, Xiong G, Benian GM, The DH-PH region of the giant protein UNC-89 activates RHO-1 GTPase in Caenorhabditis elegans body wall muscle, J. Mol. Biol. 383 (2008) 747–752. [PubMed: 18801371]

[40]. Wisniewski EO, Mistriotis P, Bera K, Law RA, Zhang J, Nikolic M, Weiger M, Tuntithavornwat S, Afthinos A, Zhao R, Kalab P, Scarcelli G, Friedl P, Konstantopoulos K, Dorsoventral polarity directs cell responses to migration track geometries, Sci. Adv. 6 (2020) eaba6505. [PubMed: 32789173]

[41]. Palazzo AF, Cook TA, Alberts AS, Gundersen GG, mDia mediates Rho-regulated formation and orientation of stable microtubules, Nat. Cell Biol. 3 (2001) 723–729. [PubMed: 11483957]

[42]. Salaycik KJ, Fagerstrom CJ, Murthy K, Tulu US, Wadsworth P, Quantification of microtubule nucleation, growth and dynamics in wound-edge cells, J. Cell Sci. 118 (2005) 4113–4122. [PubMed: 16118246]

[43]. Matov A, Applegate K, Kumar P, Thoma C, Krek W, Danuser G, Wittmann T, Analysis of microtubule dynamic instability using a plus-end growth marker, Nat. Methods 7 (2010) 761–768. [PubMed: 20729842]

[44]. Guardia T, Eason M, Kontrogianni-Konstantopoulos A, Obscurin: a multitasking giant in the fight against cancer, Biochim. Biophys. Acta Rev. Canc 1876 (2021) 188567.

[45]. Rahib L, Wehner MR, Matrisian LM, Nead KT, Estimated projection of US cancer incidence and death to 2040, JAMA Netw Open 4 (2021), e214708. [PubMed: 33825840]

Author Manuscript Author Manuscript Author Manuscript Author Manuscript

[46]. Neoptolemos JP, Kleeff J, Michl P, Costello E, Greenhalf W, Palmer DH, Therapeutic developments in pancreatic cancer: current and future perspectives, Nat. Rev. Gastroenterol. Hepatol. 15 (2018) 333–348. [PubMed: 29717230]

[47]. Hocker JR, Postier RG, Li M, Lerner MR, Lightfoot SA, Peyton MD, Deb SJ, Baker CM, Williams TL, Hanas RJ, Discriminating patients with early-stage pancreatic cancer or chronic pancreatitis using serum electrospray mass profiling, Cancer Lett. 359 (2015) 314–324. [PubMed: 25637792]

[48]. Perry NA, Vitolo MI, Martin SS, Kontrogianni-Konstantopoulos A, Loss of the obscurin-RhoGEF downregulates RhoA signaling and increases microtentacle formation and attachment of breast epithelial cells, Oncotarget 5 (2014) 8558. [PubMed: 25261370]

[49]. Ridley AJ, Schwartz MA, Burridge K, Firtel RA, Ginsberg MH, Borisy G, Parsons JT, Horwitz AR, Cell migration: integrating signals from front to back, Science 302 (2003) 1704–1709. [PubMed: 14657486]

[50]. Wittmann T, Waterman-Storer CM, Cell motility: can Rho GTPases and microtubules point the way? J. Cell Sci. 114 (2001) 3795–3803. [PubMed: 11719546]

[51]. Stehbens S, Wittmann T, Targeting and transport: how microtubules control focal adhesion dynamics, J. Cell Biol. 198 (2012) 481–489. [PubMed: 22908306]

[52]. Lee EY, Muller WJ, Oncogenes and tumor suppressor genes, Cold Spring Harb Perspect Biol 2 (2010) a003236. [PubMed: 20719876]

[53]. Nobis M, Herrmann D, Warren SC, Kadir S, Leung W, Killen M, Magenau A, Stevenson, Lucas MC, Reischmann N, Vennin C, Conway JRW, Boulghourjian A, Zaratzian A, Law AM, Gallego-Ortega D, Ormandy CJ, Walters SN, Grey ST, Bailey J, Chtanova T, Quinn JMW, Baldock PA, Croucher PI, Schwarz JP, Mrowinska A, Zhang L, Herzog H, Masedunskas A, Hardeman EC, Gunning PW, Del Monte-Nieto G, Harvey RP, Samuel MS, Pajic M, McGhee EJ, Johnsson AE, Sansom OJ, Welch HCE, Morton JP, Strathdee D, Anderson KI, Timpson P, A RhoA-FRET biosensor mouse for intravital imaging in normal tissue homeostasis and disease contexts, Cell Rep. 21 (2017) 274–288. [PubMed: 28978480]

Author Manuscript Author Manuscript Author Manuscript Author Manuscript

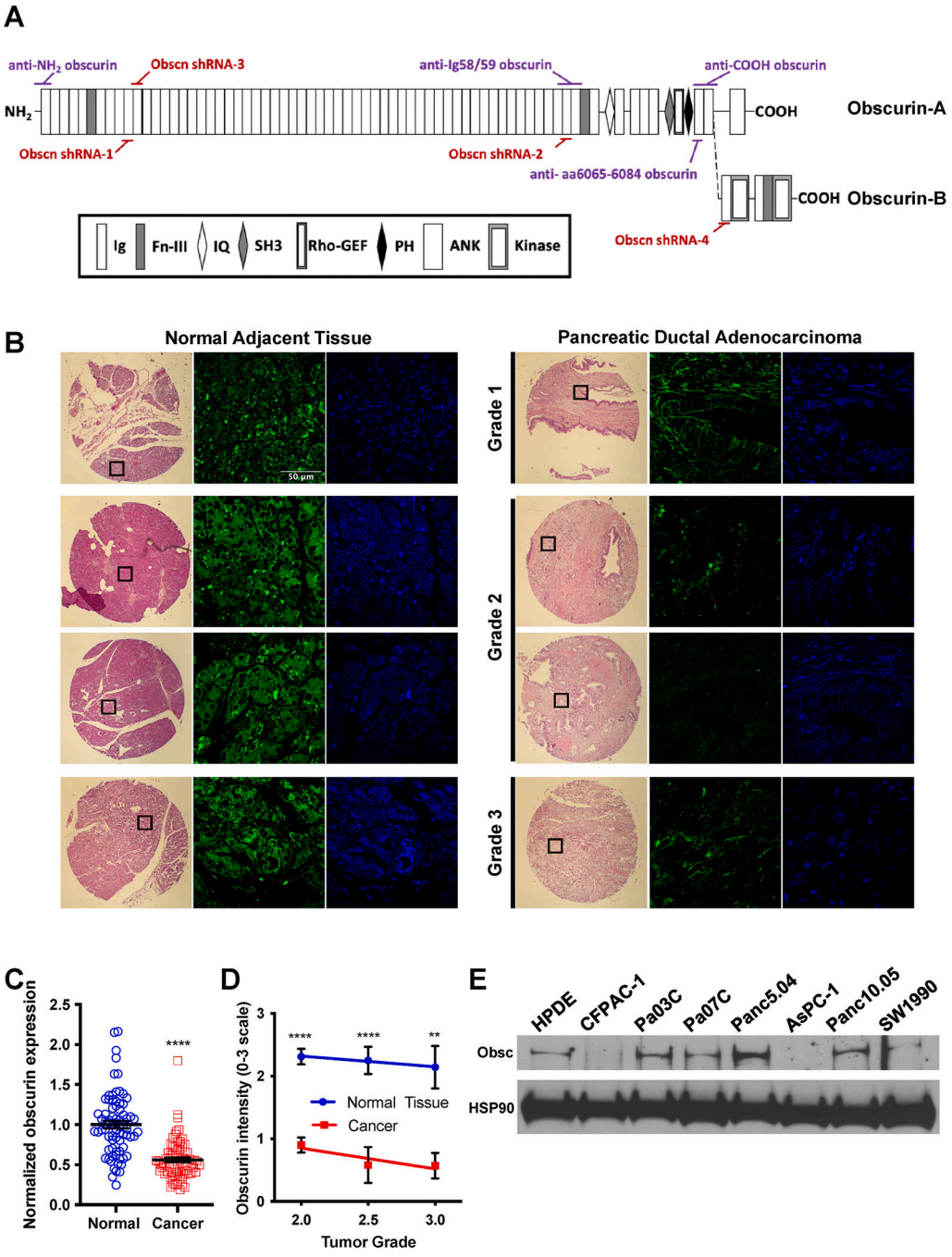

Fig. 1. Obscurin expression is markedly reduced in human PDAC relative to pancreatic epithelial tissue.

(A) Schematic of giant obscurins A and B showing their domain composition as well as the regions targeted by antibodies and shRNAs. shRNA-1, shRNA-2 and shRNA-3 target both giant obscurin A and B, while shRNA-4 targets specifically obscurin-B. **(B)** Representative images of tissue biopsies of grade 1 through 3 pancreatic adenocarcinoma and matched normal tissues. Hematoxylin and eosin (H&E) stained images display a boxed region (left) which was imaged using confocal (right) after staining with the obscurin Ig 58/59 antibody

Author Manuscript Author Manuscript Author Manuscript Author Manuscript

(green) and DAPI (blue). **(C)** Obscurin expression levels were quantified across the entire tissue specimens and values of pancreatic tumor biopsies were normalized to those of adjacent normal tissues for each matched pair. Data represent mean ± S.E.M from 75 tumor specimens and matched normal adjacent tissues. ****$p < 0.0001$ using Student's t-test after log transformation. **(D)** Obscurin levels were graded in each tissue sample based on signal intensity on a scale ranging from 0 (absent), 1 (low), 2 (medium) to 3 (high), and plotted as a function of the tumor grade. Data represent mean ± S.E.M. **$p < 0.01$ and ****$p < 0.0001$ using two-way ANOVA followed by Šídák multiple comparisons test. Data analysis for grades 1 and 1/2 were not included because of the low number of these biopsies in tumor microarray. **(E)** Immunoblot showing the expression of obscurin isoforms in normal human pancreatic ductal epithelial (HPDE) cell line and pancreatic cancer cell lines (CFPAC-1, Pa03C, Pa07C, Panc5.04, AsPC-1, Panc10.05 and SW1990) using the obscurin Ig 58/59 antibody.

Author Manuscript Author Manuscript Author Manuscript Author Manuscript

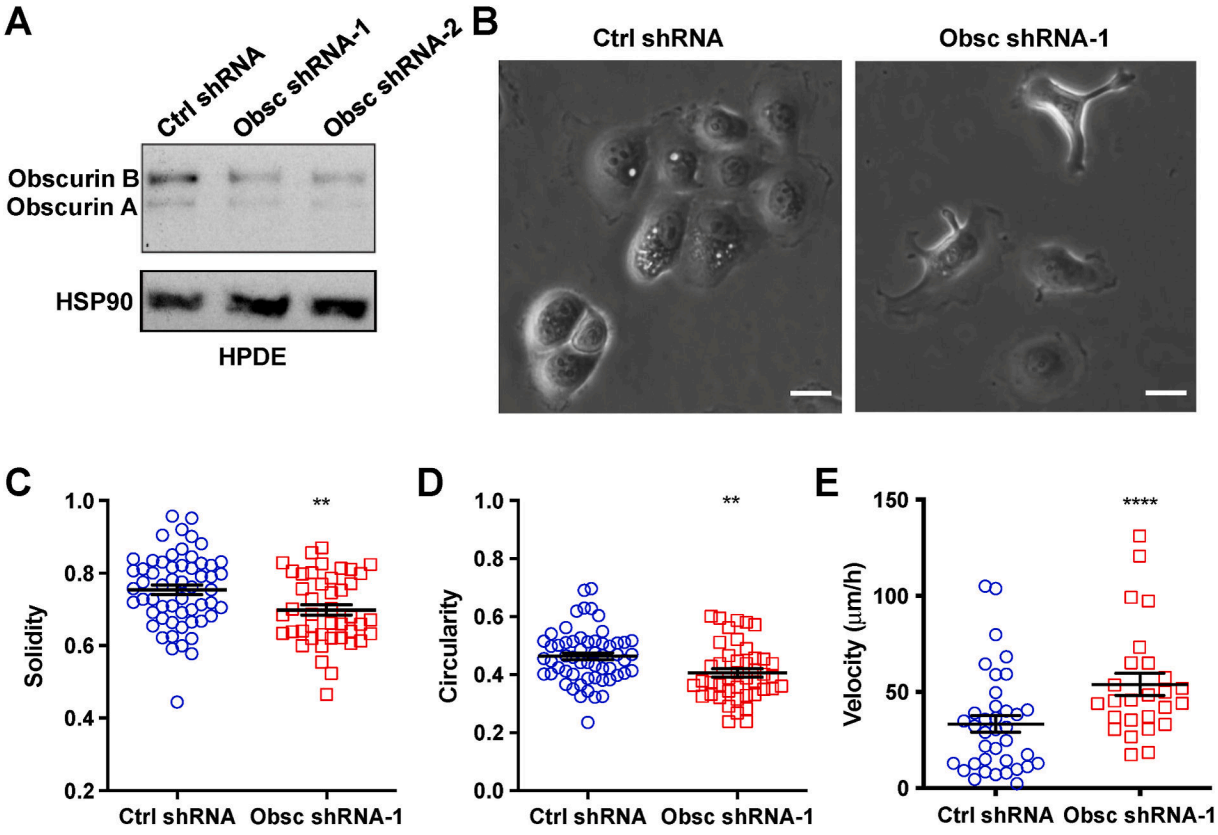

Fig. 2. Knockdown of giant obscurins in human pancreatic ductal epithelial HPDE cells enhances motility.

(A) Giant obscurins A and B are downregulated in HPDE cells following transfection with obscurin shRNA-1 or -2 compared to control shRNA. **(B)** Representative phase-contrast images of scramble control- and obscurin shRNA-1- expressing HPDE cells plated on a 2D surface. Scale bar: 50 μm. **(C)** The solidity and **(D)** circularity of obscurin shRNA-1-depleted and control shRNA HPDE cells that exited 10 × 10 μm^2 microchannels into a 2D-like collagen I-coated substrate. Data represent mean ± S.E.M. for n ≥ 44 cells from three independent experiments. **(E)** Migration velocity of obscurin shRNA-1-depleted and control shRNA HPDE cells inside 10 × 10 μm^2 collagen I-coated microchannels. Data represent mean ± S.E.M. for n = 26–37 cells from three independent experiments. **p < 0.01 and ****p < 0.0001 using Student's t-test for normal distributions (C, D) or after log transformation (E).

Author Manuscript
Author Manuscript
Author Manuscript
Author Manuscript

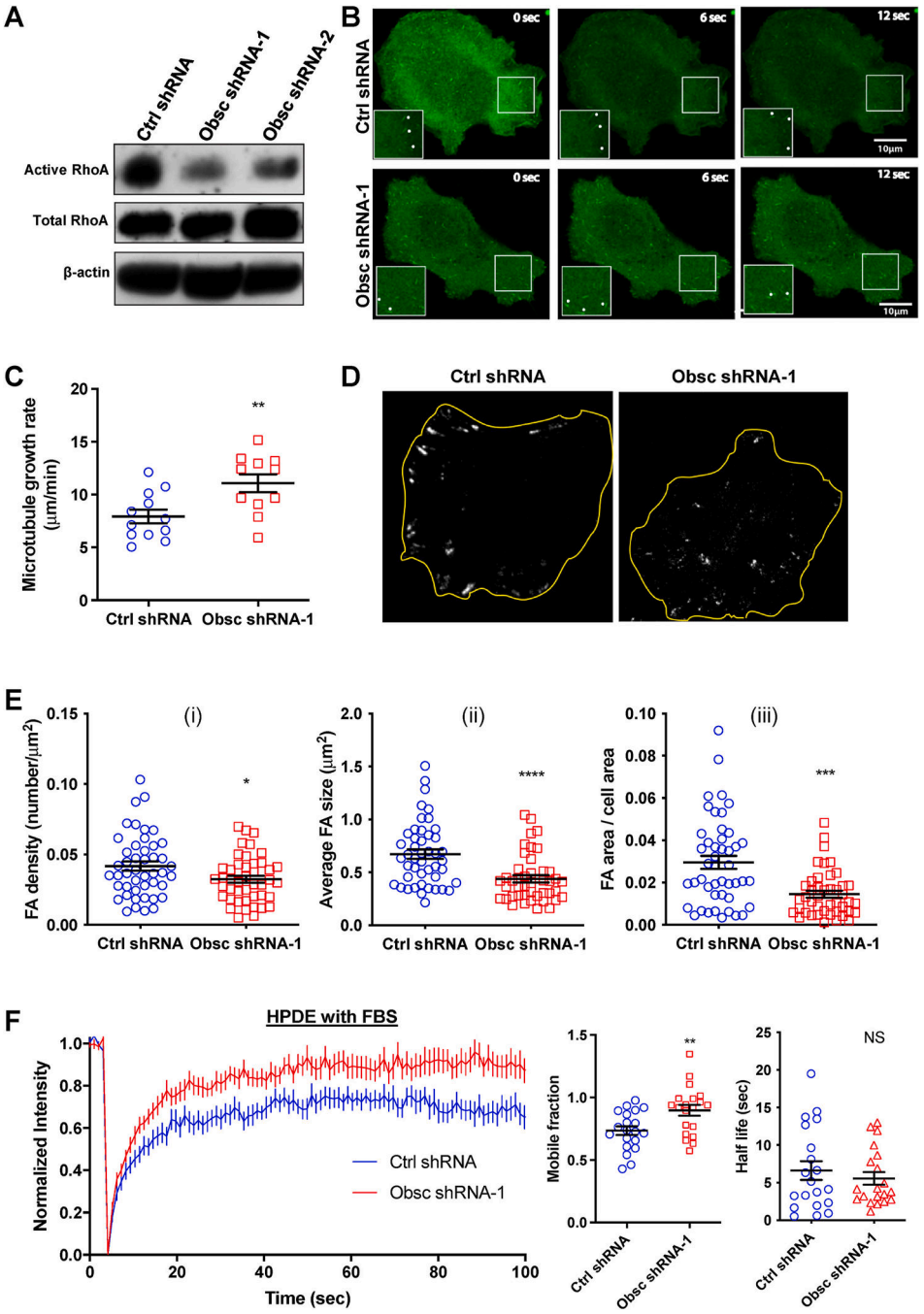

Fig. 3. Obscurin-depleted HPDE cells display reduced RhoA activity, faster microtubule and actin dynamics and decreased FA density and size.

(A) Representative pull-down assays showing active and total RhoA in scramble control and obscurin shRNA-1- and shRNA-2-expressing HPDE cells. β-actin and total RhoA were used as loading controls. **(B)** Time lapse images showing EB1-GFP comets in scramble control and obscurin-shRNA-1 HPDE cells. White dots indicate growing microtubules. **(C)** Effect of control shRNA and obscurin shRNA-1 on microtubule growth rate of EB1-GFP-expressing HPDE cells. **(D)** Representative TIRF microscopy images of control and obscurin shRNA-1-

Author Manuscript Author Manuscript Author Manuscript Author Manuscript

expressing HPDE cells stained with pY-paxillin to visualize FAs. The cell boundary is traced in yellow. **(E)** Average focal adhesion density per area (i), average focal adhesion size (ii) and the average focal adhesion area per cell area (iii). **(F)** FRAP analysis of Lifeact-RFP-expressing scramble control and obscurin shRNA-1 HPDE cells in the presence of 10% FBS, and quantification of mobile fraction and half-life of actin recovery. Data represent mean ± S.E.M. for ≥11 cells (C) or ≥44 cells (E) or ≥20 cells (F) from 3 independent experiments. *$p < 0.05$, **$p < 0.01$, ***$p < 0.001$, and ****$p < 0.0001$ using Student's t-test for normal distributions (C, Ei, F) or after log transformation (Eii-iii). All experiments were performed on 2D collagen I-coated surfaces.

Author Manuscript Author Manuscript Author Manuscript Author Manuscript

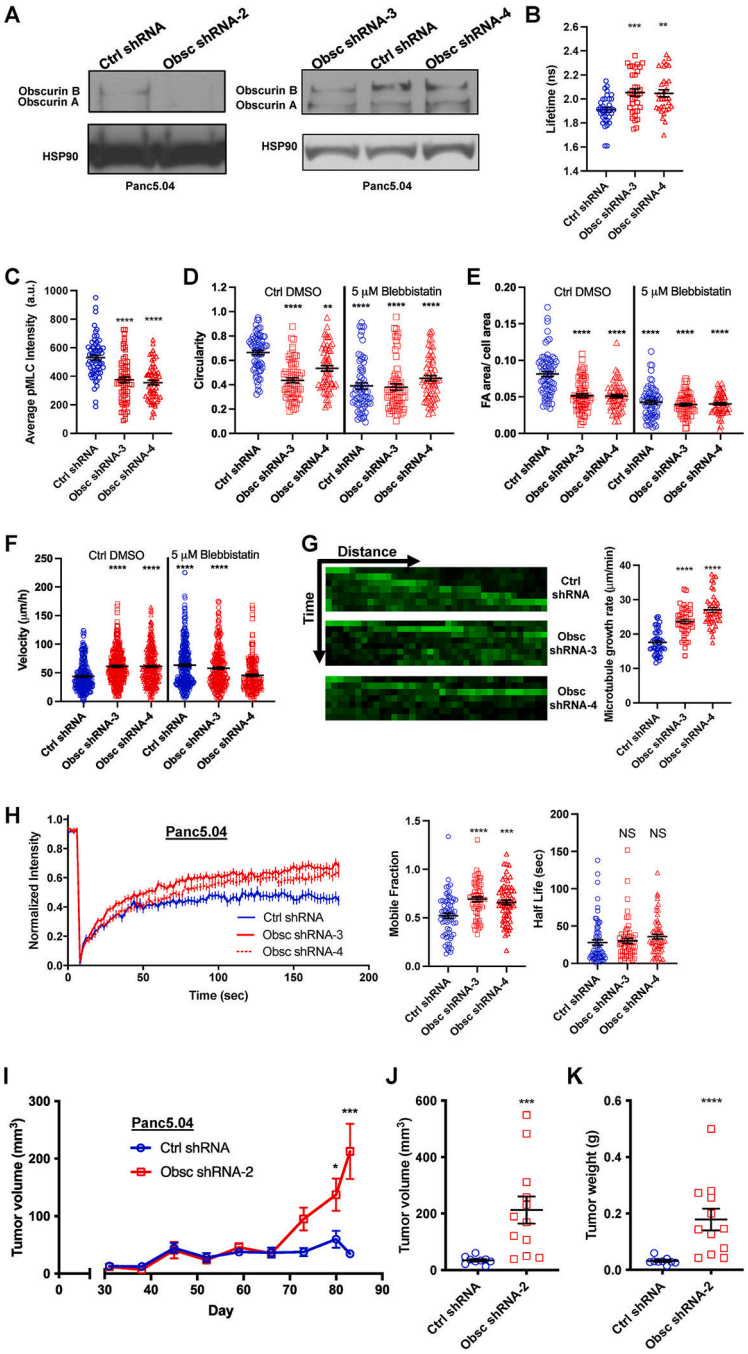

Fig. 4. Knockdown of giant obscurins in Panc5.04 pancreatic cancer cells promotes faster migration *in vitro* via cytoskeletal remodeling and increases tumor growth *in vivo*.

(A) Expression of giant obscurins in Panc5.04 cells after transfection with control or obscurin shRNA-2 followed by clonal selection or using the lentiviral technology for shRNA-3/-4. **(B)** Donor fluorescence lifetime of RhoA activity biosensor on 2D as measured by FLIM-FRET. Data represent mean ± S.E.M. for n ≥ 32 cells from three independent experiments. **(C)** Average pMLC intensity (a.u.) of control, obscurin shRNA-3 and shRNA-4 Panc5.04 cells. Data represent mean ± S.E.M. for n ≥ 61 cells from 3 independent

Author Manuscript Author Manuscript Author Manuscript Author Manuscript

experiments. Effect of partial inhibition of cell contractility with low concentration of blebbistatin (5 μM) on **(D)** cell circularity and **(E)** focal adhesions on 2D as well as **(F)** migration velocity inside 10 × 10 μm^2 microchannels for scramble control and obsucrin-KD cells. Data represent mean ± S.E. M. for n ≥ 63 cells (D,E) or n ≥ 205 cells (F) from 3 to 4 independent experiments. **(G)** Kymographic analysis and microtubule growth rate of EB1-GFP-expressing control versus obscurin-knockdown Panc5.04 cells. Data represent mean ± S.E.M. for n ≥ 42 cells from 3 experiments. **(H)** FRAP analysis of β-actin-GFP-expressing scramble control and obscurin shRNA-3/-4 Panc5.04 cells in the presence of 10% FBS, and quantification of mobile fraction and half-life of actin recovery. Data represent mean ± S.E.M. for n ≥ 61 cells from 3 experiments. **(I)** Quantification of tumor volume in mice following subcutaneous implantation of scramble control and obscurin shRNA-2 Panc5.04 cells as a function of time. *In vivo* growth of scramble control and obscurin shRNA-2 Panc5.04 cells in a subcutaneous injection model, as assessed by **(J)** the volume and **(K)** weight of tumors harvested postmortem. Data represent the mean ± S.E.M. 9–12 mice. *p < 0.05, **p < 0.01, ***p < 0.001 and ****p < 0.0001 relative to control shRNA were determined using one-way ANOVA followed by Tukey's post-hoc test (B,C,E,G,H), or Kruskal-Wallis followed by Dunn's multiple comparisons test (D,F), or two-way ANOVA followed by Šídák multiple comparisons test (I), or Student's t-test after log transformation (J, K). NS: non-significant.

Author Manuscript Author Manuscript Author Manuscript Author Manuscript

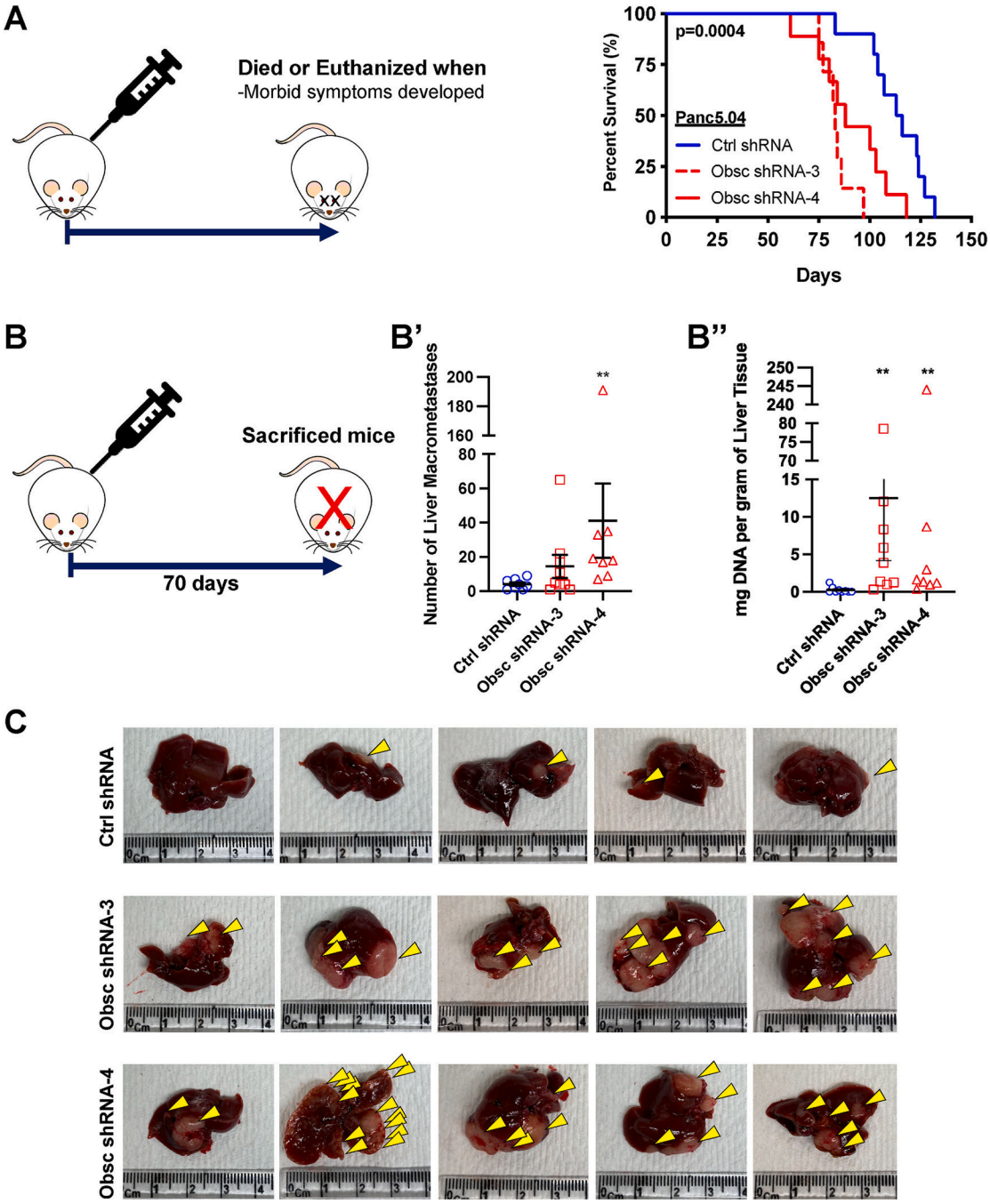

Fig. 5. Depletion of giant obscurins in Panc5.04 reduces survival by promoting metastasis *in vivo*.

(A) NSG mice, injected with scramble control, obscurin shRNA-3 or shRNA-4 Panc5.04 cells using the hemispleen injection technique, were monitored over time and euthanized when they exhibited morbid symptoms. Kaplan-Meier survival curves of NSG mice were compared using log-rank (Mantel-Cox) test. **(B)** NSG mice were sacrificed 70 days post hemispleen injection with control or obscurin-knockdown Panc5.04 cells, and **(B′)** the number of visible liver macrometastasis foci and **(B′′)** human DNA detected on the harvested livers of mice were quantified. Data represent mean ± S.E.M. *p <0.05 and

Author Manuscript Author Manuscript Author Manuscript Author Manuscript

p <0.01 were determined using Kruskal-Wallis followed by Dunn's multiple comparisons test. In (B"), the mean ± S.E.M. for shRNA-4 is 32.7 ± 30.2 mg of human DNA per gram of liver tissue. **(C) Gross anatomical pictures of representative livers harvested from mice injected with scramble control (top row) or obscurin-knockdown (middle and bottom rows) Panc5.04 cells. Yellow arrowheads indicate visible liver macrometastases.